IEEE Access
Multidisciplinary ⋮ Rapid Review ⋮ Open Access Journal

Received May 10, 2022, accepted May 23, 2022, date of publication June 1, 2022, date of current version June 8, 2022.

Digital Object Identifier 10.1109/ACCESS.2022.3179475

Transparent Saltwater in Glass Structure: Simultaneous Tunable UHF Antenna and EMI Shielding Window

DUY TUNG PHAN, (Member, IEEE), TIEN DAT NGUYEN, AND CHANG WON JUNG, (Senior Member, IEEE)

Graduate School of NID Fusion Technology, Seoul National University of Science and Technology, Seoul 139-746, South Korea

Corresponding author: Chang Won Jung (changwoj@seoultech.ac.kr)

This work was supported by the National Research Foundation of Korea Grant funded by the Korean Government under Grant 2016R1D1A1B02012957.

ABSTRACT This paper presents a transparent saltwater in glass structure working simultaneously as a tunable UHF antenna and EMI shielding window. The proposed structure has high transparency (>91%), which is achieved through its use of salty water as a conductive medium held within a clear and hollow glass rectangular prism, allowing its use as an optical window. On one hand, the saltwater in glass structure plays a role as an EMI shielding window with a shielding effectiveness (SE) above 20 dB in the C-band. On the other hand, the proposed structure works as a frequency-and beam-tunable UHF antenna by using dual-port feeding configurations. Experimental results show that for a basic configuration using single-port feeding, the antenna has a −6 dB bandwidth ranging from 350 to 680 MHz and efficient radiation efficiency (>60%) over the band. For advanced configurations, a tunable frequency and directional radiation pattern can be achieved with enhancing gain compared to the basic configuration. These results demonstrate the proposed antenna can be used as a bi-functional device, i.e., as a tunable antenna and EMI shielding window. To the best of our knowledge, this is the first demonstration of such a bi-functional device with transparent performance.

INDEX TERMS Transparent antenna, EMI shielding window, saltwater, tunable antenna, UHF antenna.

I. INTRODUCTION

Currently, broadcasting applications have become very popular and play an important role in delivering multimedia services to users through mobile or handheld devices [1]. Most broadcasting applications such as television now operate on the ultra-high-frequency (UHF) band. However, the UHF band is one of the most challenging bands for antenna design because antennas that operate on this band are normally large, which therefore limits their practical applications [1], [2]. To overcome this problem, our idea is to design a highly optical transparency (OT) external antenna using saltwater as a transparent liquid conductor. Due to the high transparency of the saltwater, the proposed antenna can overcome the size issue that affects conventional UHF antennas without many conformity or aesthetic problems while also serving as an observation window in the construction industry at the same time. Generally, many types of solid transparent antennas have been extensively studied using a solid transparent thin film such as indium tin oxide [2], graphene [3], multilayer film [4], a metal mesh [5], or a conductive fabric [6], [7]. In terms of conformability, the antenna in [7] is fabricated using a highly flexible PDMS-conductive fabric composite. The reconfigurability is achieved by activating and deactivating the slots using PIN diodes. However, the metal mesh, multilayer film, and conductive fabric have relatively low average transparency (<80%) in the visible band from 400 to 700 nm, whereas the graphene has high sheet resistance and indium tin oxide is expensive because the cost of the rare-earth indium component [2]–[5]. With the low transparency, most previous transparent antennas are designed to work at a high frequency to reduce the size to fit specific applications, such as their installation onto the windshields of vehicles [4].

Due to its great optical transparency (OT) (>95% at a salinity level of 40 ppt), low cost, and ready availability, saltwater has recently been explored as a potential candidate for developing a new class of high-transparent antennas [8]. For transparent antennas, saltwater as the conductive part

The associate editor coordinating the review of this manuscript and approving it for publication was Shah Nawaz Burokur.

conducts electric charges in the form of ions. So far, many different types of saltwater antennas have been reported [8]–[17]. In one study [8], a basic broadband water monopole was demonstrated, and the performance of the antenna was investigated by dissolving salt in pure water. In order to improve the performance of the antenna in [8], one study in [9] introduces a feeding probe loaded with a nut and washer. Another sea-water monopole [10], [11] utilized the insertion of a dielectric base between the water and ground plane to maximize the bandwidth. In other work [12], a high-efficiency seawater monopole with an average radiation efficiency above 60% is proposed for maritime wireless communications from 40 to 200 MHz. However, saltwater, on the other hand, has a low conductivity; therefore, most existing saltwater antennas use a cylindrical structure to reduce the ohmic loss and improve radiation efficiency [11], [12], [14]–[17]. It should be noted that by using the cylindrical structure, the light arrives at the antenna not only at a normal but also at an oblique incidence angle; therefore, the transparency of the antenna is significantly reduced due to strong reflection and refraction occur. To overcome this problem, in previous work [13] we presented a planar saltwater dipole antenna with very high optical transparency. However, a dipole antenna with a feeding point between two arms is not feasible as a window because the connectors are not transparent. On the other hand, the rapid development of wireless technologies such as mobile and satellite communications give rise to an unwanted and undesirable EM wave, i.e., EM interference (EMI). The EMI is a common issue for electronic components used in various industries, including military, defense, and aerospace etc. [18]–[20]. Therefore, the EMI shielding technologies become more urgent to protect. Highly conductive materials such as metallic copper that are typical of EMI shielding materials, however, they are opaque materials which limits transparent applications. Meanwhile, a typical transparent conductive material such as indium tin oxide (ITO) is very limited for the EMI shielding due to the trade-off between the optical transparencies and shielding effectiveness [19].

In this paper, we present a highly transparent structure which can work simultaneously as a tunable UHF antenna and EMI shielding window. The high transparency of the structure is achieved using salty water held within a clear and hollow glass rectangular prism as a conductive medium. On one hand, the structure can be used as an EMI shielding window due to the saltwater layer acts as an EM radiation barrier. On the other hand, we add RF feeding sources connect with the saltwater layer as conductive part and window frame as ground plane making the structure can work as a tunable antenna. Two advanced configurations of the antenna with two feeding ports are also proposed to achieve frequency-and beam-tunable characteristics and to enhance the gain of the antenna. The measured results demonstrate that the proposed structure can be used as a bi-functional device, i.e., as a UHF-tunable antenna and an EMI shielding window.

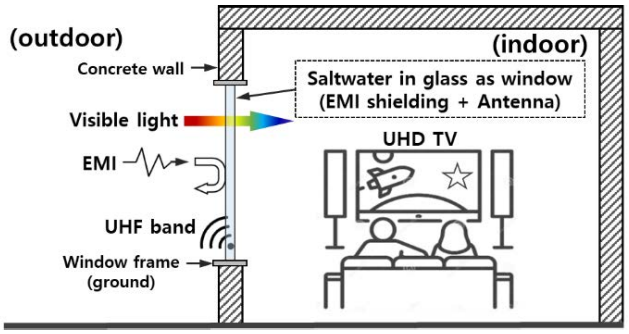

FIGURE 1. Conceptual illustration of the transparent liquid-based window simultaneously playing as UHF antenna and EMI shielding.

II. CONCEPT AND SCHEMATIC

Fig. 1 illustrates the concept of the transparent saltwater in glass structure that can work simultaneously as a tunable UHF antenna and EMI shielding window. Due to its high optical transparency, the structure allows visible light to pass through unchanged; therefore, it can alternate as a conventional window. On one hand, the conductive salty water layer of proposed structure will serve as a radiation barrier to block EM interference from outside so that the radiation essentially cannot penetrate to interfere with electronics in the room. On the other hand, the proposed structure can be used as antenna to transmit/receive desire RF waves for certain wireless communication applications, e.g., the UHF band for broadcast television applications. This approach is not only simple but also meets aesthetical requirements and is therefore feasible for use in many practical applications. It should be noted that due to the tunable-characteristic of the liquid antenna, it could be developed to work at other different frequencies for wireless communications and other important spectrums. This paper is an initial work on that kind of bi-functional device; therefore we demonstrate with the UHF band as an example. Schematic of proposed structure when it works as a transparent liquid antenna with different configurations is shown in Figs. 2(a)-(c). In the basic configuration, as shown in Fig. 2(a), the transparent liquid antenna is fed by a single port and a thin metal strip on the top of the feeding probe for better excitation [8]. It should be noted that the metal strip is placed inside the glass container and is separated from the ground plane the glass layer to avoid short circuited. However, the single-port configuration usually shows a low gain and cannot easily achieve tunable characteristics. Therefore, we propose advanced configurations using dual port feeding, as shown in Figs. 2(b) and (c). It should be noted that in all configurations, the window frame plays as the ground planes of the antenna. As shown in Fig. 2(b), two ports are arranged opposite each other along the z-axis. In this way, two ground planes can be hidden in the upper and lower edges of the window frame without any effect on the transparency. By changing the phases of two these ports, we can control the current distribution on the antenna; therefore,

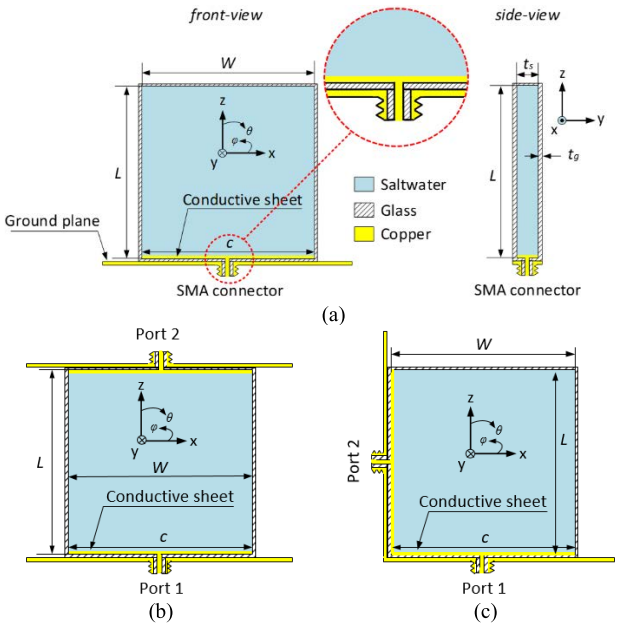

FIGURE 2. Schematic of the transparent liquid antenna under different configurations: (a) single feeding port (left: front-view, right: side-view), (b) dual opposite feeding ports, and (c) dual orthogonal feeding ports.

TABLE 1. Optimized dimensions of the liquid antenna. (Unit: millimeters.)

Parameter	W	c	t_g	L	t_s
Value (mm)	15	15	1	15	3

we expect to achieve frequency-tunable characteristic and an omnidirectional radiation. We also propose another advanced configuration with ports 1 and 2 arranged along the z-axis and x-axis, respectively. As shown in Fig. 2(c), two ground planes also exist on the left side and lower edge of the window frame and do not cause any aesthetic problems. With this proposed configuration, we expect to achieve a directional radiation pattern.

Normally, a saltwater antenna shows relatively low radiation efficiency due to the high ohmic loss of the saltwater [13]. Therefore, in the next sections, first we investigate the optical and electrical performance capabilities of saltwater with different salinity levels. Secondly, we conduct a parametric study to optimize the performance of the basic configuration by means of port feeding. Thirdly, the performance outcomes of the advanced configurations of the antenna are investigated. Finally, measurements are carried out to validate the simulation findings.

III. OPTICAL AND SHIELDING ANALYSIS

A. OPTICAL AND CONDUCTIVITY OF SALTWATER

Fig. 3 depicts the measured conductivity and optical transparency of saltwater at various salinity levels ranging from 35 to 200 parts per thousand (ppt). The conductivity is measured using a portable electrical conductivity meter,

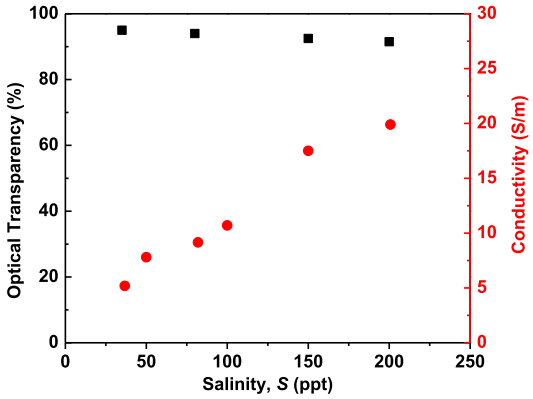

FIGURE 3. Measured optical transparency (black squares) and conductivity (red circles) of saltwater corresponding to different salinity levels at room temperature.

while the optical transparency is carried out using a UV/VIS spectrophotometer connected to a computer. It should be noted that optical transparency in Fig. 3 is the average value in the visible band.

As illustrated in Fig. 3, when the salinity rises, the conductivity rises rapidly while the optical transparency falls slightly. It is also reported in a previous study by the authors [8], [13], under certain temperature and pressure conditions, the conductivity of saltwater increases with an increase in the salinity level. However, the salinity of saltwater at a certain point reaches its saturation limit, meaning that the conductivity of saltwater is limited. Under ambient conditions, the maximum salinity of saltwater at 263 parts per thousand (ppt) corresponds to conductivity of 25 S/m. To prevent the saltwater from becoming saturated, we use saltwater at 200 ppt for our antenna design. This salinity level ensures that conductivity of the saltwater remains as high as 20 S/m with a very high optical transparency of 91.5%.

B. EMI SHIELDING ANALYSIS

First, we theoretically analysis the EMI shielding effectiveness (SE) of the proposed structure using plane-wave shielding theory [21]. We assume that the saltwater as a conductive layer will mainly contribute of shielding effectiveness of the structure. Therefore, the shielding of the proposed structure can be theoretically determined as:

$$EMISE = 20\log\frac{\eta_0}{4\eta_{sw}} + 20\log e^{t_{sw}/\delta_{sw}} \tag{1}$$

where η_0 and η_{sw} are intrinsic impedance of free space and saltwater layer ($\eta_0 = 377\Omega$); t_{sw} and δ_{sw} are thickness and skin-depth of the saltwater, respectively. The $\eta_{sw} = \sqrt{2\pi f\mu/\sigma_{sw}}$ and $\delta_{sw} = 1/\sqrt{\pi f\mu\sigma_{sw}}$ are the functions of conductivity of saltwater (σ_{sw}) and frequency (f). In (1), the first component is the attenuation due to the reflection of power at the interfaces whereas the second term is the attenuation due to power converted to heat as the wave propagates

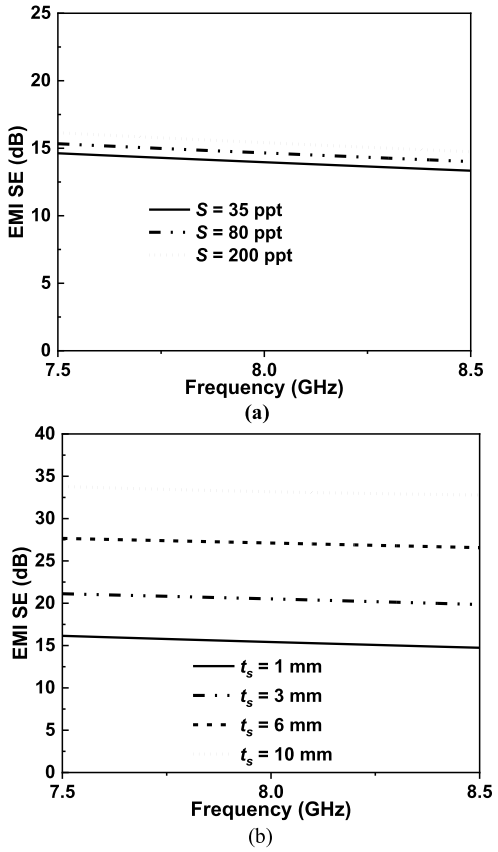

FIGURE 4. Shielding effectiveness of the saltwater in glass structure with (a) different salinity levels, (b) different thickness of the saltwater layer.

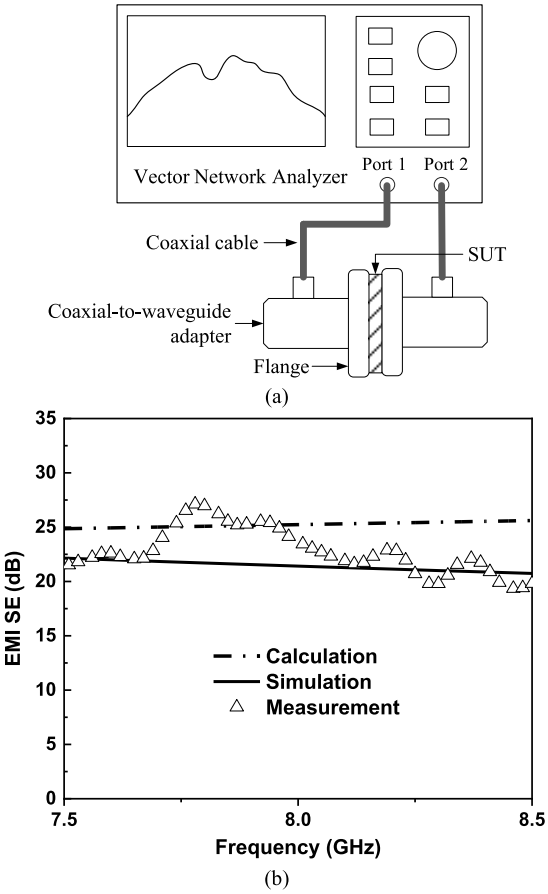

FIGURE 5. a) EMI SE measurement setup and (b) measured EMI SE of the saltwater in glass structure in comparison with the theoretical calculation and simulation.

through the structure. Using (1), the total EMI SE of proposed structure is calculated.

Then, the EMI SE of the proposed structure was investigated by simulation and then verified by measurement. The simulation was conducted using ANSYS HFSS. We use the saltwater properties which are available in the library of the HFSS, however, the conductivity is modified to the experimental values. The SE the structure is investigated at different salinity (S) and thickness (t_s) of saltwater layer to study the effect of these key parameters on its shielding performance as shown in Fig. 4. Fig. 4(a) shows the SE of the proposed structure from 7.5 to 8.5 GHz with salinity of the ASA structure changes from 35 to 200 ppt, whereas both thicknesses of the glass and saltwater layers were fixed at 1 mm. Results revealed that the SE of the proposed structure increased as the salinity increased. By combining the results in Figs. 3 and 4(a), it can be concluded that the higher the conductivity, the better shielding performance achieved for the ASA structure. Fig. 4(b) shows the SE of the structure as a function of saltwater layer thickness in the band. In this simulation, we fixed the salinity at 200 ppt and changed the thickness of the saltwater layer to investigate the shielding behaviour of the structure. The proposed structure's EMI SE increased with the increase in saltwater layer thickness from 1 to 10 mm.

To verify the simulated shielding performance, the Measurement of the structure under test (SUT) is conducted using a pair of waveguide-to-coaxial adapters, as shown in Fig. 5(a). The SUT consists of a saltwater layer with a thickness and salinity of 3 mm and 200 ppt, respectively which is held between two clear quartz glass layers ($t_g = 1$ mm, $\varepsilon = 4.3$, $\tan\delta = 0$). The SE can be determined from the power transmission coefficient (S_{21}) in dB as $SE = |S_{21}|$, which is measured using a vector network analyzer connected to the adapters, as shown in Fig. 5(a). Fig. 5(b) shows the calculated, simulated, and measured EMI SE of the SUT which is in good agreement between them. The SUT shows a measured SE above 20 dB with an average value of 23.5 dB in the band.

IV. TUNABLE UHF LIQUID-BASED ANTENNA

A. SIMULATION RESULTS

Due to the liquid amount between two glass layers is kept unchanged to ensure the shielding level, therefore, we use different feeding configurations to achieve the tunable characterization for the proposed structure when it works as an antenna. This section will go through bellow order: first, the single feeding port configuration is presented; second, dual port feeding configurations (also called

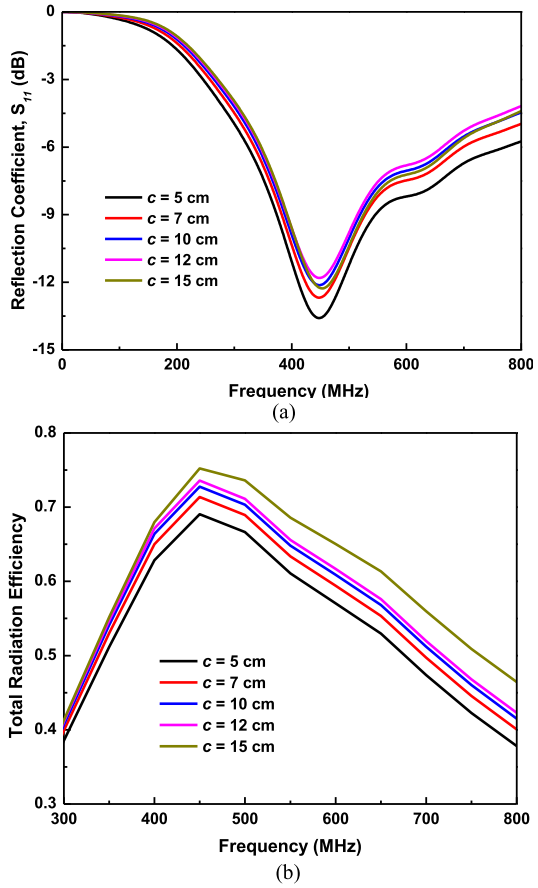

FIGURE 6. (a) Reflection coefficient and (b) total radiation efficiency of the proposed antenna with different widths of the metal sheet.

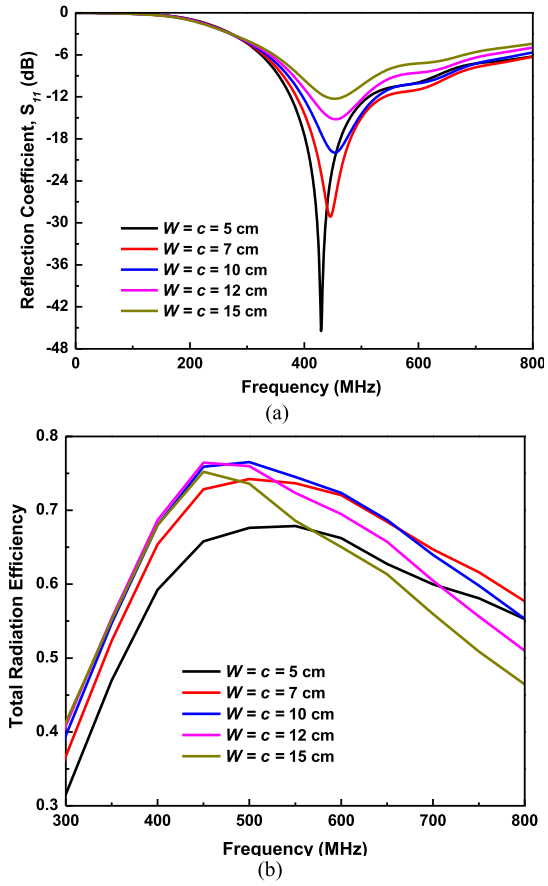

FIGURE 7. (a) Reflection coefficient and (b) radiation efficiency of the proposed antenna with different widths of the antenna and metal sheet.

advanced configurations) including opposite and orthogonal postures are carried out.

As we aforementioned, a transparent liquid antenna usually has low radiation efficiency compared to a typical metal antenna due to its higher ohmic loss. Therefore, it is important to understand the mechanism and optimize the radiation efficiency of the liquid antenna. The radiation of an antenna can be defined as in (2).

$$\eta = \frac{R_{rad}}{R_{rad} + R_{loss}} \tag{2}$$

where R_{rad} and R_{loss} are correspondingly the radiation resistance and loss resistance of the antenna. Because the antenna is a monopole type, $R_{rad} = 73\Omega$ [22]. The loss resistance can be determined from the conductivity of saltwater (σ) and from the dimension of the antenna, as expressed by (3).

$$R_{loss} = \frac{L}{\sigma W t_s} \tag{3}$$

where L, W, and t_s are the length, width, and thickness of the saltwater layer, respectively.

The (1) and (2) show that the radiation efficiency of the saltwater antenna can be enhanced when σ and t_s are increased. However, the conductivity of saltwater is limited as we are aforementioned whereas the increasing of t_s leads to a heavy window design. Therefore, we have fix the t_s at 3 mm that ensures an EMI SE above 20 dB. In additional, a metal strip is loaded on the top of the feeding probe (see Fig. 2) to improve the excitation of the antenna [8]; and the antenna's dimensions, such as the length of the metal strip (c) and the width of the antenna (W) are optimized to maximize the antenna's efficiency. It worthy to note that the metal strip is very thin (thickness 0.05 mm) and therefore does not affect the transparency of the antenna.

Fig. 6 shows the reflection coefficient and total radiation efficiency of the single-port transparent liquid antenna when the length of the metal strip varies from 5 to 15 cm. As shown in Fig. 6(a), when c increases, the resonant characteristics of the antenna do not have much of an effect and the impedance matching level is slightly poorer. However, the radiation efficiency of the antenna is significantly improved when c increases from 5 to 15 cm, as shown in Fig. 6(b). This occurs because the metal strip acts as a radiator, which contributes to an increase in the total radiation efficiency of the proposed liquid antenna. Therefore, the length of the metal strip is kept as long as the width (W) of the saltwater antenna to maximize its efficiency.

Fig. 7 shows the resonant characteristics and radiation efficiency of the liquid antenna when its width varies from

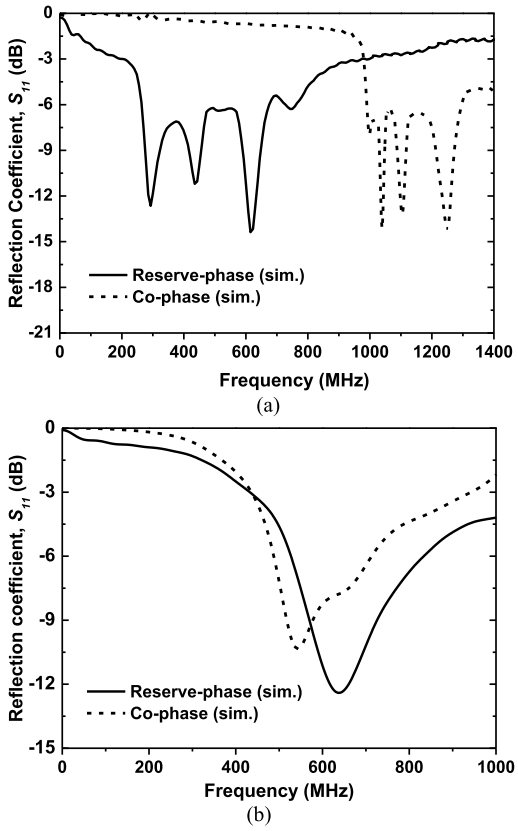

FIGURE 8. Reflection coefficient of the transparent liquid antenna with dual co-phase port feeding and dual reserve-phase port feeding: (a) two ports opposite, and (b) two ports orthogonal.

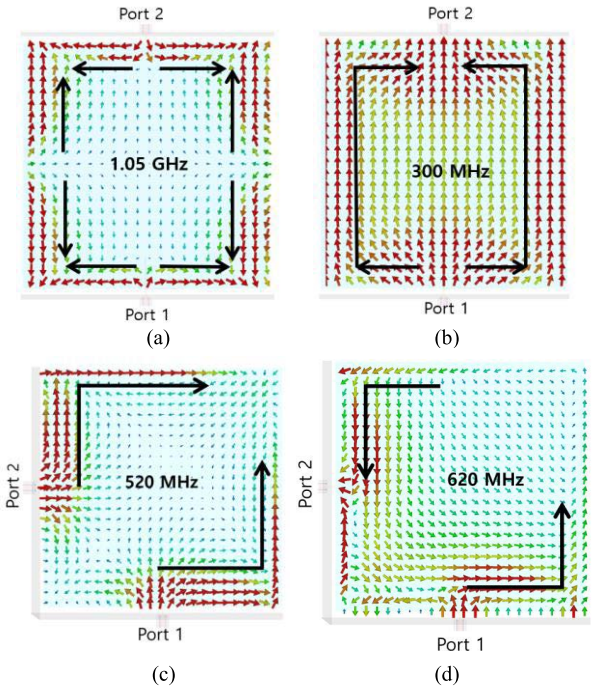

FIGURE 9. Surface current distribution at the resonant frequencies of the transparent liquid antenna: (a) opposite ports, co-phase feeding, (b) opposite ports, reserve-phase, (c) two orthogonal ports, co-phase, and (d) two orthogonal ports, reserve-phase.

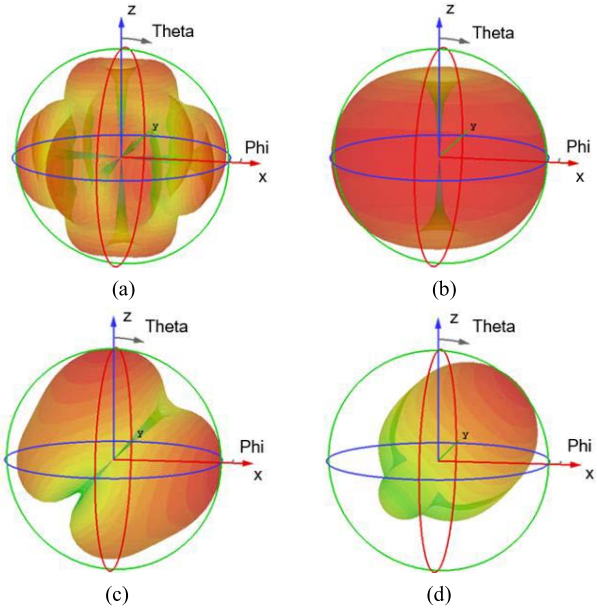

FIGURE 10. 3D radiation pattern of the transparent liquid antenna with (a) opposite ports, co-phase feeding; (b) opposite ports, reserve-phase feeding; (c) orthogonal ports, co-phase feeding; and (d) orthogonal ports, reserve-phase feeding.

5 to 15 cm. We can observe from Fig. 7(a) that the resonant frequency of the antenna does not change much, whereas the impedance matching level is significantly improved when W increases. On the other hand, when W increases from 5 to 15 cm, the radiation efficiency of the antenna also increases significantly (Fig. 7(b)) despite the fact that the impedance matching becomes poorer with an increase in W. This likely stems from the ohmic loss of the antenna, which decreases when W increases. However, we can also observe from Fig. 7(b) that the total radiation efficiency of the antenna increases rapidly with W below 10 cm and that it increases slowly when W exceeds 10 cm. Therefore, in this study, we chose $W = c = 15cm$ as the optimum dimensions of the antenna. The optimum dimensions of the antenna are listed in Table 1. It worthy to note that this is an initial work on this kind of bi-functional device and length and width of the structure seem small that may limit its application as a window. Therefore, we are aiming to extend our work with bigger size structure for broader use cases.

Figs. 8(a) and (b) correspond to the configuration with two ports arranged opposite to each other along the z-axis (see Fig. 2(b)) and arranged orthogonally along the z-axis and x-axis (see Fig. 2(c)), respectively. For each configuration, two ports are fed in a co-phase and reserve-phase configuration relative to each other in an effort to investigate their resonant characteristics.

As shown in Fig. 8(a), when we change from the co-phase feeding mode to the reserve-phase feeding mode, the resonant frequency of the antenna moves from the higher band to the lower band. However, in the configurations where the two

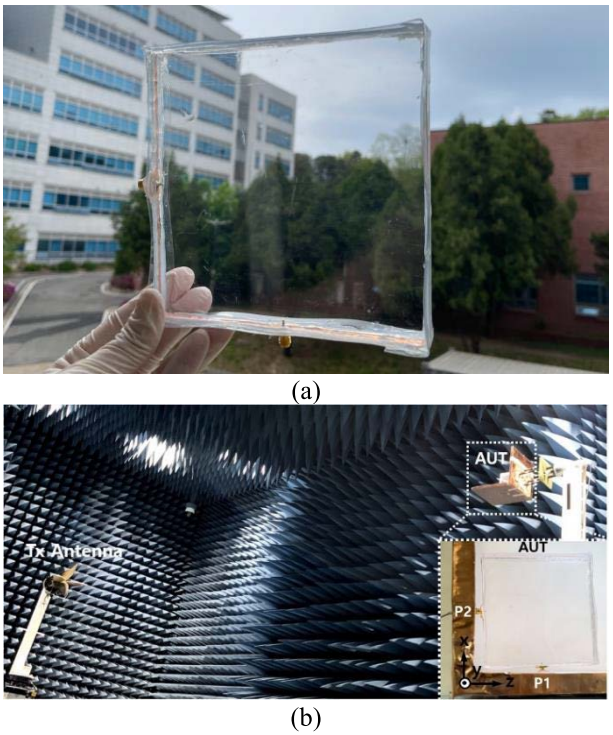

FIGURE 11. (a) Fabricated antenna, and (b) Measurement setup of the transparent liquid antenna in an anechoic chamber (the inset shows a closer look of the antenna under test (AUT)).

ports are arranged orthogonally, we can observe a reserve trend because the resonant frequency of the antenna moves from a lower to a higher band when we change from reserve-phase feeding to co-phase feeding. Therefore, both configurations demonstrate that a tunable frequency can be realized by the interchange between co-phase feeding to reserve-phase feeding. However, the configuration with opposite ports shows a much wider frequency-tunable range compared to the configuration with orthogonal ports, making it a more suitable configuration for frequency-tunable purposes.

In order to understand the mechanism associated with the resonant characteristics of the two advanced configurations, the current distributions at the resonant frequencies of the configurations are assessed at the resonant frequencies, as shown in Fig. 9. In each case, two ports are also fed in the co-phase and reserve-phase configurations relative to each other. It is well-know that a longer current will introduces a lower resonant frequency and vice versa. In Fig. 9, we use the length of arrows to indicate the length of currents. As shown in Fig. 9(a), the current is distributed into different short segments with different directions, demonstrating that the antenna is working at a higher resonance level. When the two ports are fed in the reserve-phase configuration, as shown in Fig. 9(b), the current is uniformly distributed along with the antenna from port 1 forward to port 2. This type of current distribution indicates that the antenna is working in the fundamental resonance condition. Therefore, the resonant frequency in this case is much lower than that of co-phase

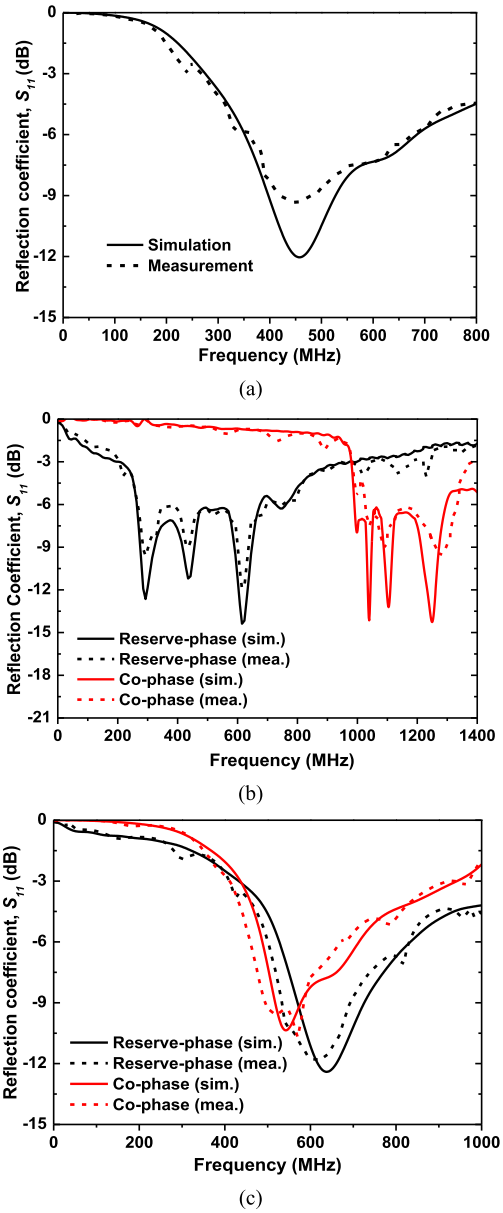

FIGURE 12. Measured reflection coefficients of the transparent liquid antenna in comparison with the simulation: (a) single feeding port, (b) opposite feeding ports, and (c) orthogonal feeding ports.

feeding in Fig. 9(a). Figs. 9(c) and (d) show the current distribution of the configuration with orthogonal feeding ports when ports 1 and 2 are fed in the co-phase and reserve-phase conditions, respectively. We find that the current distribution in these cases is quite similar, indicating that both cases are operating at the fundamental resonance. The length of the current in Fig. 9(c) is slightly longer than that in Fig. 9(d), resulting in the resonant frequency of co-phase feeding being slightly lower than in reserve-phase feeding, as shown in Fig. 9(b).

Fig. 10 shows the simulated 3D radiation pattern of the transparent liquid antenna with different advanced configurations and feeding phases. By using opposite feeding

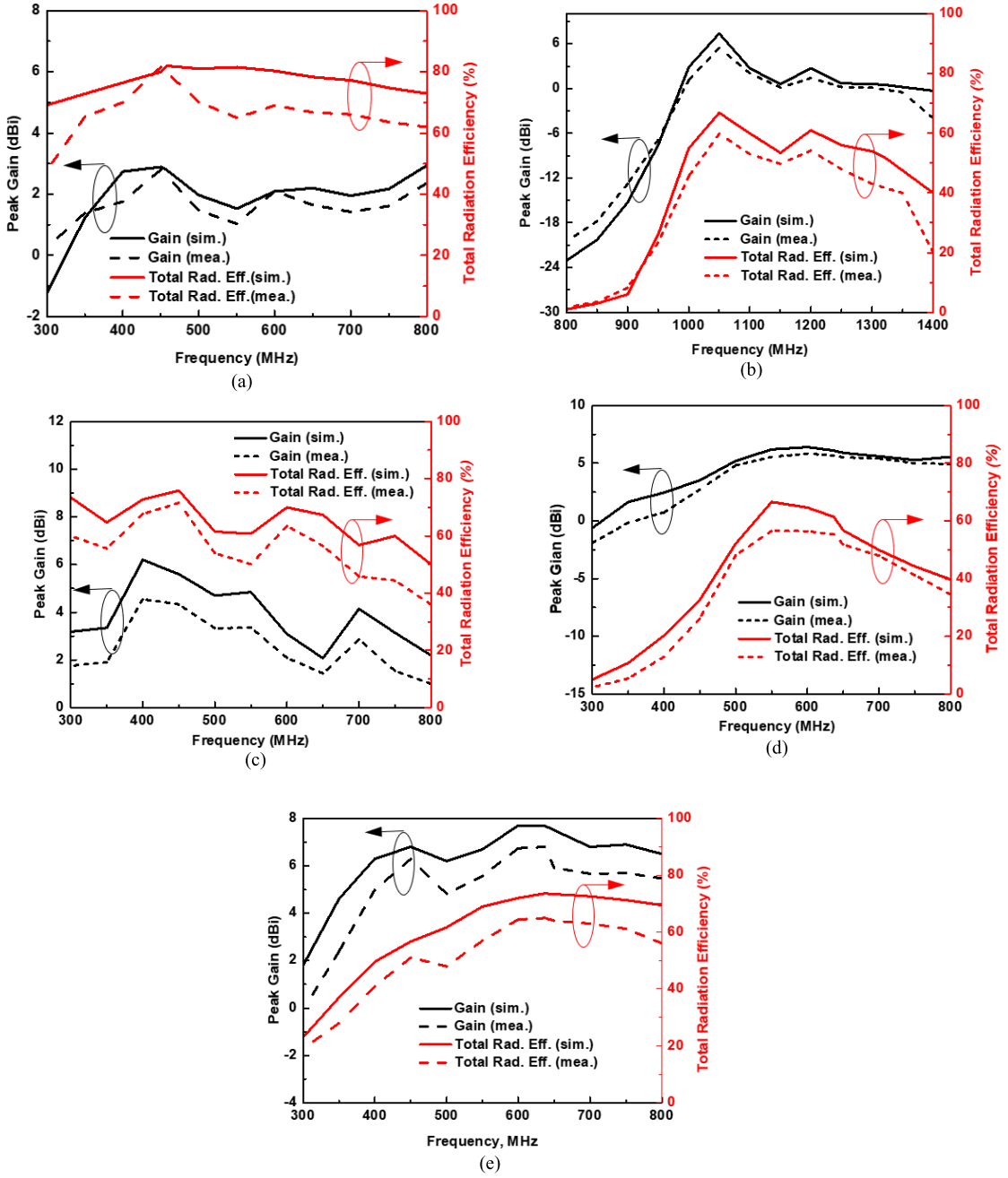

FIGURE 13. Measured gain and total radiation efficiency of the transparent liquid antennas: (a) single port feeding; (b) opposite ports, co-phase feeding; (c) opposite ports, reserve-phase feeding; (d) orthogonal ports, co-phase feeding; and (e) orthogonal ports, reservephase feeding.

ports, the antenna acts as an omnidirectional antenna (Figs. 10(a) and (b), whereas it shows directional radiation characteristics when two feeding ports are arranged orthogonally to each other, as shown in Figs. 10(c) and (d). This result shows that the configuration with opposite feeding ports can be used for broadcasting applications such as television while the configuration with orthogonal feeding ports is more suitable for applications that require a high-directivity antenna, such as satellite communications.

B. MEASUREMENT RESULTS AND DISCUSSION

Fig. 11(a) shows the fabricated saltwater in glass structure with feeding so that it can work as an antenna. We can observe a very high optical transparency is still maintained. Fig. 11(b) shows a far-field measurement in an anechoic chamber using the NSI-2000 measuring equipment. The inset image in Fig. 11(b) depicts the fabricated transparent liquid antenna (advanced configuration), where the two feeding ports are orthogonally arranged along the x- and z-axis. We find that

the fabricated antenna retains its very good transparency. Figs. 12 shows the simulated and measured reflection coefficients. The measured S_{11} is assessed using a network analyzer E5071B, with the findings in good agreement with the simulation results. As shown in Fig. 12(a), the transparent liquid antenna with single-port feeding (see Fig. 2(a)) shows a very wide −6 dB bandwidth ranging from 350 to 680 MHz (of 330 MHz; 64%). This frequency nearly covers the band for ultra-high-definition TV (UHD TV) applications. The reflection coefficient of the antenna with feeding using two opposite (see Fig. 2(b)) is shown in Fig. 12(b). As expected, the resonant frequency of the antenna moves significantly to a higher band when we change from the reserve-phase feeding to the co-phase feeding configuration. It was observed that the antenna in the reserve-phase configuration shows a wide −6 dB bandwidth ranging from 260 to 750 MHz (490 MHz; 97%), while the resonant band of the co- phase configuration is much higher, from 1.03 to 1.32 GHz (290 MHz; 24.6%). This result demonstrates that frequency-tunable characteristics of the transparent liquid antenna can be achieved by feeding a different phase between two opposite ports. Fig. 12(c) presents the simulated and measured reflection coefficients of an antenna with a feeding configuration of two orthogonal ports (see Fig. 2(c)). For the configuration with orthogonal ports, the antenna shows a small left-shift of the resonant frequency from 600 to 550 MHz when we change from reserve-phase to co-phase feeding. The −6dB bandwidths of the antenna in the reserve-phase and co-phase configurations are 330 MHz (500 to 830 MHz; 49.6%) and 240 MHz (460 to 700 MHz; 41.3%), respectively.

Fig. 13 depicts the simulated and measured gain and the total radiation efficiency of the transparent liquid antenna. The antenna in the basic configuration with a single port shows typical performance outcomes with the average gain and total radiation efficiency on the UHF band being 1.73 dBi and 69%, respectively (Fig. 13(a)). As shown in Figs. 13 (b), the antenna in the advanced configuration with two opposite co-phase ports feeding shows an efficiency rate as high as 63% with an average value of 58.8% and gain up to 5.4 dBi on the resonant band from 1.03 to 1.32 GHz. Meanwhile, as shown in Fig. 13(c), the feeding configuration with the two opposite reserve-phase ports exhibits higher efficiency up to 71% and lower gain levels up to 4.5 dBi compared to the co-phase feeding configuration. This can be explained by the radiation characteristic of the antenna in the co-phase feeding configuration, which is more directive than that of the reserve-phase configuration, as shown in Figs. 9(a) and (b). Figs. 13(d) and (e) show the gain and efficiency of the antenna when two ports are arranged orthogonally. We find that the co-phase and reserve-phase feeding configuration exhibit similar average gain and efficiency outcomes over the resonant bands. The average gains of the co-phase and reverse-phase configurations are 5.8 and 6.8 dBi, respectively, whereas the corresponding average efficiency rates are 56% and 60%. The simulated and measured radiation patterns of the proposed antenna with different feeding configurations are depicted in Fig. 14. We observed good agreement between the simulation and measurement outcomes. As shown in Fig. 14(a), the antenna shows an omnidirectional radiation pattern on the xoy-plane, while it acts

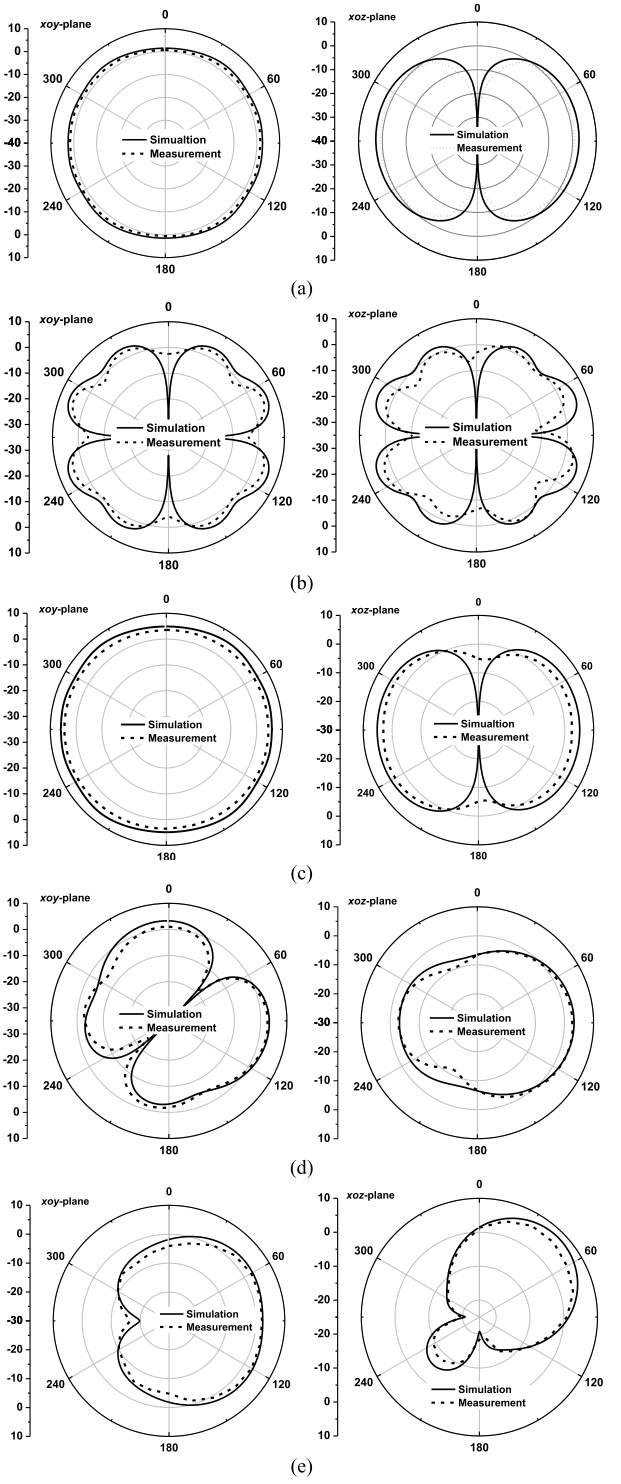

FIGURE 14. Measured radiation pattern of the transparent liquid antennas on the xoy-and xoz-planes: (a) single port feeding; (b) opposite ports, co-phase feeding; (c) opposite ports, reserve-phase feeding; (d) orthogonal ports, co-phase feeding; and (e) orthogonal ports, reserve-phase feeding.

as a directional antenna on the xoz-plane. The radiation pattern of a conventional metal monopole. Figs. 14 (b) and (c) show the radiation pattern of the antenna with two opposite co-phase and reserve-phase feeding ports at their resonant frequencies, respectively. Both configurations exhibit omni-directional radiation characteristics. However, we find that the co-phase configuration is operating at a higher resonance level while the reserve-phase configuration acts as a typical dipole at the fundamental resonance level. On the other hand, the antenna using two orthogonal feeding ports shows directional radiation patterns, as presented in Figs. 14 (d) and (e). This result demonstrates that a tunable radiation pattern can be achieved by changing from the configurations with single and two opposite feeding ports to that with orthogonal feeding ports.

TABLE 2. Performance comparison between the proposed structure with reported transparent antenna/emi shielding.

Ref	Center frequency (*GHz*)	OT (%)	Antenna performance		Shielding performance
			Gain (*dBi*)	Eff. (%)	EMI SE (*dB*)
[8]	2.65/-	85	2.3	71	-
[12]	0.063/-	N/A	N/A	61.3	-
[14]	1.5/-	N/A	0.1	50	-
[19]	-/2.45	68.4	-	-	31.4
[20]	-/10	45	-	-	82
[24]	-/15	91	-	-	26
This work	0.6/8	91.5	1.73	69	23.5

Table 2 gives performance comparison between the proposed bi-functional structures with existing transparent antennas/EMI shielding structures. It should be note that the comparison is given separately because most of reported transparent devices, to best our knowledge, are neither antenna nor EMI shielding structures. As shown in Table 2, the proposed structure shows a highest OT with good antenna and EMI performance among the reported works so far.

V. CONCLUSION

This paper presented a highly optical transparent saltwater in glass structure which can work as a tunable UHF antenna and EMI shielding window at the same time. The proposed structure uses a salty water layer as conductive medium, which is held within a clear and hollow glass rectangular prism. The overall optical transparency of the structure is over 91%. On one hand, the structure shows a shielding effectiveness (SE) above 20 dB in the C-band allowing it to be used as an EMI shielding window. On the other hand, we add RF feeding sources connect with the saltwater layer as conductive part and utilize window frames as ground planes making the structure can work as a tunable antenna. To improve the radiation efficiency of the antenna, a thin metal strip was loaded into a feeding probe to achieve greater excitation. Advanced configurations of the antenna with two feeding ports are also proposed to achieve frequency-tunable characteristics and to enhance the gain of the antenna. Measurement results show that for the basic configuration with a single feeding port, the antenna has a −6 dB bandwidth from 350 to 680 MHz and efficient radiation efficiency (>60%) over the band. For advanced configurations, tunable characteristics or a directional radiation pattern can be achieved with an enhanced gain compared to that of the basic configuration. These results demonstrate that the proposed structure can be used as a bi-functional device, i.e., as a tunable UHF antenna and an EMI shielding window. It is also worth to note that one of most concerns regarding to water-based antennas is how to guarantee the performance under extremely temperature conditions in winter since salty water will be frozen. In this case, some anti-frozen liquid such as propylene glycol (PG) could be added to lower the freezing point up to −55°C [25]. This problem will be carefully investigated in our future works

REFERENCES

[1] C. J. Wang and Y. L. Lee, "A compact dipole antenna for DTV applications by utilizing L-shaped stub and coupling strip," *IEEE Trans. Antennas Propag.*, vol. 62, no. 12, pp. 6515–6519, Dec. 2014.
[2] P. D. Tung and C. W. Jung, "Optically transparent wideband dipole and patch external antennas using metal mesh for UHD TV applications," *IEEE Trans. Antennas Propag.*, vol. 68, no. 3, pp. 1907–1917, Mar. 2020.
[3] S. Kosuga, S. Nagata, S. Kuromatsu, R. Suga, T. Watanabe, O. Hashimoto, and S. Koh, "Optically transparent antenna based on carrier-doped three-layer stacked graphene," *AIP Adv.*, vol. 11, no. 3, Mar. 2021, Art. no. 035136.
[4] Y. Kim, C. Lee, S. Hong, C. W. Jung, and Y. Kim, "Design of transparent multilayer film antenna for wireless communication," *Electron. Lett.*, vol. 51, no. 1, pp. 12–14, Aug. 2015.
[5] M. Inomata, T. Sayama, T. Motegi, O. Kagaya, H. Shoji, S. Takeuchi, and K. Nobuoka, "Transparent glass antenna for 28 GHz and its signal reception characteristics in urban environment," in *Proc. 14th Eur. Conf. Antennas Propag. (EuCAP)*, Mar. 2020, pp. 1–5.
[6] A. S. M. Sayem, R. B. V. B. Simorangkir, K. P. Esselle, D. N. Thalakotuna, and A. Lalbakhsh, "An electronically-tunable, flexible, and transparent antenna with unidirectional radiation pattern," *IEEE Access*, vol. 9, pp. 147042–147053, 2021.
[7] B. Mohamadzade, R. B. V. B. Simorangkir, R. M. Hashmi, R. Gharaei, A. Lalbakhsh, S. Shrestha, M. Zhadobov, and R. Sauleau, "A conformal, dynamic pattern-reconfigurable antenna using conductive textile-polymer composite," *IEEE Trans. Antennas Propag.*, vol. 69, no. 10, pp. 6175–6184, Oct. 2021.
[8] D. T. Phan and C. W. Jung, "Optically transparent sea-water monopole antenna with high radiation efficiency for WLAN applications," *Electron. Lett.*, vol. 55, no. 24, pp. 1269–1271, Nov. 2019.
[9] H. Fayad and P. Record, "Broadband liquid antenna," *Electron. Lett.*, vol. 42, no. 3, pp. 177–178, Feb. 2006.
[10] E. Paraschakis, H. Fayad, and P. Record, "Ionic liquid antenna," in *Proc. IEEE Int. Workshop Antenna Technol., Small Antennas Novel Metamater. (IWAT)*, Mar. 2005, pp. 552–554.
[11] L. Xing, Y. Huang, S. S. Alja'afreh, and S. J. Boyes, "A monopole water antenna," in *Proc. Loughborough Antennas Propag. Conf. (LAPC)*, Nov. 2012, pp. 1–4.
[12] C. Hua, Z. Shen, and J. Lu, "High-efficiency sea-water monopole antenna for maritime wireless communications," *IEEE Trans. Antennas Propag.*, vol. 62, no. 12, pp. 5968–5973, Dec. 2014.
[13] P. Duy Tung and C. W. Jung, "Highly transparent planar dipole using liquid ionized salt water under surface tension condition for UHD TV applications," *IEEE Trans. Antennas Propag.*, vol. 69, no. 1, pp. 35–42, Jan. 2021.
[14] L. Xing, Y. Huang, Y. Shen, S. Alja'afreh, Q. Xu, and R. Alrawashdeh, "Further investigation on water antennas," *IET Microw., Antennas Propag.*, vol. 9, no. 8, pp. 735–741, Jun. 2015.
[15] L. Xing, J. Zhu, Q. Xu, D. Yan, and Y. Zhao, "A circular beam-steering antenna with parasitic water reflectors," *IEEE Antennas Wireless Propag. Lett.*, vol. 18, no. 10, pp. 2140–2144, Oct. 2019.

[16] C. Hua and Z. Shen, "Shunt-excited sea-water monopole antenna of high efficiency," *IEEE Trans. Antennas Propag.*, vol. 63, no. 11, pp. 5185–5190, Sep. 2015.
[17] Z. Peng, X. Liang, W. Zhu, J. Geng, C. He, Y. Yao, Y. Qian, and R. Jin, "Metal-loaded seawater antenna with high radiation efficiency and wide-band characteristics," *IEEE Antennas Wireless Propag. Lett.*, vol. 16, pp. 1671–1674, 2017.
[18] S. B. Kondawar and P. R. Modak, "Theory of EMI shielding," in *Materials for Potential EMI Shielding Applications*, K. Joseph, R. Wilson, and G. George, Eds. Amsterdam, The Netherlands: Elsevier, 2020, ch. 2, pp. 9–25.
[19] P. D. Tung and C. W. Jung, "High optical visibility and shielding effectiveness metal mesh film for microwave oven application," *IEEE Trans. Electromagn. Compat.*, vol. 62, no. 4, pp. 1076–1081, Aug. 2020.
[20] M. M. Masud, B. Ijaz, I. Ullah, and B. Braaten, "A compact dual-band EMI metasurface shield with an actively tunable polarized lower band," *IEEE Trans. Electromagn. Compat.*, vol. 54, no. 5, pp. 1182–1185, Oct. 2012.
[21] R. B. Schulz, V. C. Plantz, and D. R. Brush, "Shielding theory and practice," *IEEE Trans. Electromagn. Compat.*, vol. 30, no. 3, pp. 187–201, Aug. 1988.
[22] R. Luebbers, L. Chen, T. Uno, and S. Adachi, "FDTD calculation of radiation patterns, impedance, and gain for a monopole antenna on a conducting box," *IEEE Trans. Antennas Propag.*, vol. 40, no. 12, pp. 1577–1583, Dec. 1992.
[23] P. D. Tung and C.W. Jung, "Optically transparent and very thin structure against electromagnetic pulse (EMP) using metal mesh and saltwater for shielding windows," *Sci. Rep.*, vol. 11, p. 2603, Jan. 2021.
[24] Y. Han, J. Lin, Y. Liu, H. Fu, Y. Ma, P. Jin, and J. Tan, "Crackle template based metallic mesh with highly homogeneous light transmission for high-performance transparent EMI shielding," *Sci. Rep.*, vol. 6, p. 25601, May 2016.
[25] L. Xing, Y. Huang, Q. Xu, S. Alja'afreh, and T. Liu, "Complex permittivity of water-based liquids for liquid antennas," *IEEE Antennas Wireless Propag. Lett.*, vol. 15, pp. 1626–1629, 2015.

DUY TUNG PHAN (Member, IEEE) received the B.S. degree in electronics and telecommunications engineering from Vinh University, Vietnam, in 2011, the M.S. degree in radio engineering from Tula State University, Russia, in 2015, and the Ph.D. degree in antenna/RF engineering from the Seoul National University of Science and Technology (SeoulTech), South Korea, in 2021.

He was a Postdoctoral Fellow at the Centre of Wireless Communications, University of Oulu, Finland, when he was a Ph.D. Student at SeoulTech. He has authored/coauthored more than 20 journal articles and conference papers in antenna/RF field. His main research interests include transparent antennas, EMI/EMC, metasurface-based polarization converters and absorbers, and reconfigurable intelligent surfaces for mmWave and sub-THz applications. He received the Best Ph.D. Award from SeoulTech in 2021.

TIEN DAT NGUYEN received the B.S. degree in electrical and electronics engineering from the Hanoi University of Science and Technology (HUST), Hanoi, Vietnam, in 2020. He is currently pursuing the M.S. degree with the Graduate School of Nano IT Design Fusion, Seoul National University of Science and Technology, Seoul, South Korea. His research interests include filters and transparent antennas.

CHANG WON JUNG (Senior Member, IEEE) received the B.S. degree in radio science and engineering from Kwangwoon University, Seoul, South Korea, in 1997, the M.S. degree in electrical engineering from the University of Southern California, Los Angeles, CA, USA, in 2001, and the Ph.D. degree in electrical engineering and computer science from the University of California at Irvine, Irvine, CA, USA, in 2005.

He was a Research Engineer with the Wireless Communication Department, LG Information and Telecommunication, Seoul, from 1997 to 1999. From 2005 to 2008, he was a Senior Research Engineer with the Communication Laboratory, Samsung Advanced Institute of Technology, Suwon, South Korea. Since 2008, he has been a Professor with the Graduate School of Nano IT Design Technology, Seoul National University of Science and Technology, Seoul. He has authored over 120 papers in refereed journals and conference proceedings, one book, and more than 50 international patents. His current research interests include antennas for multi-mode multi-band communication systems, multifunctional reconfigurable antennas, electromagnetic interference/electromagnetic compatibility, millimeter-wave applications, and wireless power transfer for energy harvesting.